Journal of Alloys and Compounds 968 (2023) 171746

Contents lists available at ScienceDirect

Journal of Alloys and Compounds

journal homepage: www.elsevier.com/locate/jalcom

NiFeP composites supported on Ni foam as an efficient and robust bifunctional electrocatalyst for overall water splitting in alkaline solution

Guofa Dong [a,b,1], Tingting Chen [a,b,1], Fengyan Xie [a,b,1], Donglin Xue [a], Tingyan Liu [a], Long Chen [a], Jianrong Xia [a], Shaowu Du [a,b,*], Fengyun Wang [c], Feng Xie [d], Johnny C. Ho [e,**]

[a] Fujian Engineering Research Centre of New Chinese Lacquer Materials, College of Materials and Chemical Engineering, Minjiang University, Fuzhou 350108, China
[b] Research Centre of Advanced Materials, Fuzhou Institute of Oceanography, Fuzhou 350108, China
[c] College of Physics, Qingdao University, Qingdao 266071, China
[d] Clothing and Design Faculty, Minjiang University, Fuzhou 350108, China
[e] Department of Materials Science and Engineering, and State Key Laboratory of Terahertz and Millimeter Waves, City University of Hong Kong, Kowloon 999077, Hong Kong Special Administrative Region, China

ARTICLE INFO

Keywords:
Overall water splitting
Hydrogen evolution reaction
Oxygen evolution reaction
Phosphide
Bifunctional electrocatalyst
Electrocatalysis

ABSTRACT

Developing high-efficiency and cost-effective bifunctional electrocatalysts for overall water splitting is crucial for the utilization of hydrogen energy. In this work, NiFeP composites supported on Ni foam were prepared by a mild, wet chemical method followed by an *in situ* phosphorization process. The as-prepared NiFeP/NF exhibits high electrocatalytic activity in hydrogen and oxygen evolution reactions, which should be attributed to the unique heterostructures in the NiFeP composite. When used as a bifunctional catalyst for overall water splitting in an alkaline solution, a long-term duration of 1100 h has been achieved under a current density of 300 mA cm^{-2}. Such good performance makes the composite a promising electrocatalyst and ranks it among the best catalysts reported recently for overall water splitting under alkaline conditions. Notably, the preparation of NiFeP/NF can be accomplished without complicated reaction conditions and using expensive instruments, which enables great potential for large-scale application.

1. Introduction

Nowadays, the energy crisis and environmental issues severely impede the future development of humankind. One imperative strategy to tackle these challenges is developing green and sustainable energy sources to replace fossil fuels gradually. Under the highest gravimetric energy density and green combustion process, hydrogen (H_2) exhibits enormous advantages, which promote it as an ideal energy carrier for the next energy revolution [1]. However, about 97% of the hydrogen in the world is still manufactured by steam reforming of natural gas or coal gasification [2,3]. There will be a yield of about 10 kg of CO_2 when producing 1 kg of hydrogen from water methane, which means a heavy dependence on fossil fuels and high emission of carbon dioxide as well as other harmful gases. Therefore, producing hydrogen with efficient and eco-friendly methods is the prime problem to solve for the widespread application of hydrogen. In recent years, as a high-efficiency and green method, electrochemical water splitting has been considered a promising technology to renewably prepare H_2 from water [4], which consumes electricity to produce hydrogen from water while no emission of any pollutants like CO_2. Today, with the decreasing cost of renewable electricity generated from solar, wind, water, and heat, there is a fast-growing interest in hydrogen production by water electrolysis. Thus, electrochemical water splitting has become an ideal technique to collect and store renewable energy, especially for better use of intermittent energy sources [3,4].

However, for a very long period, electrochemical water splitting was regarded as a worthless technology for industrial hydrogen production because of its low economic efficiency rate and high electricity consumption, which should be attributed to its sluggish reaction kinetics caused by the high energy barriers. To trigger and operate the

* Corresponding author at: Fujian Engineering Research Centre of New Chinese Lacquer Materials, College of Materials and Chemical Engineering, Minjiang University, Fuzhou 350108, China.
** Corresponding author.
E-mail addresses: swdu@mju.edu.cn (S. Du), johnnyho@cityu.edu.hk (J.C. Ho).
[1] These authors contributed equally.

https://doi.org/10.1016/j.jallcom.2023.171746
Received 22 April 2023; Received in revised form 8 August 2023; Accepted 13 August 2023
Available online 14 August 2023

electrochemical water-splitting process, sufficiently high voltages must be applied, which is not economical and heavily hinders industrial deployment. Theoretically, the water electrolysis process consists of two half-reactions which are the oxygen evolution reaction (OER) on the anode and the hydrogen evolution reaction (HER) on the cathode [5]. High-performance electrocatalysts are greatly desired to overcome the slow and complicated kinetics of the reactions. Numerous studies have been carried out in recent years, and a few highly efficient electrocatalysts have been developed [6,7]. The most effective electrocatalysts for commercial applications are noble metals, such as Pt, Ru, and Ir, or their composites [8]. However, high prices and low reserves on the earth largely obstruct the common utilization of noble-metal catalysts. Therefore, exploring efficient, stable, low-cost, and abundant catalysts for electrochemical water splitting is imperative for efficiently utilizing hydrogen energy. Recently various transition metal-based electrocatalysts, such as oxides [9–11], hydroxides [12,13], chalcogenide [14,15], phosphides [16–18], nitrides [19,20], carbides [21,22] and MOFs [23,24], have been well investigated for water splitting. Among them, transition metal-based phosphides (TMPs) are considered as one of the most promising catalysts for commercial use because of their low overpotential on HER and OER, tunable electronic properties, high electrical conductivity, and low cost [25,26]. Notably, TMPs are often used as bifunctional catalysts for both HER and OER [27], which is meaningful and cost-effective for hydrogen production from water.

Of the TMPs, NiFe-based phosphides have recently attracted widespread research interests because of their superior performance on both OER and HER [28,29], as well as the abundant reserves of Ni and Fe on earth. To boost the intrinsic activity of the NiFe-based TMPs, various strategies, such as element doping, vacancy defects, amorphization, and construction of heterostructures, were used to modulate electronic structures [30–32]. He and his co-workers prepared NiFeP electrocatalysts with rich defects (d-NiFeP/CC) by defect engineering, and good performance was achieved [33]. To deliver a current density of 10 mA cm^{-2}, the overpotentials needed for HER, OER, and overall water splitting were just 88, 185, and 256 mV, respectively. *In situ* Raman analysis and theoretical calculations demonstrated that the defects of d-NiFeP catalysts could significantly accelerate the reconstruction of the neighbor nickel atoms to generate highly active NiOOH species, which would greatly enhance the OER kinetics. Li et al. constructed NiFeP/NiFe-LDH heterojunctions coupled with graphene oxide by interfacial engineering [34]. The optimized catalyst ($Ni_{0.7}Fe_{0.3}P$/LDH/GO) achieved ultra-low overpotential values of 79 mV for HER and 198 mV for OER at a current density of 10 mA·cm^{-2}. They attributed the enhanced performance to improved electronic conductivity, enlarged electrochemically active area, and accelerated kinetics. Moreover, constructing hollow structures, porous structures, arrays, sheets, or nanowires has been used to optimize the microstructures of the NiFe-based TMPs [35–37], which could greatly increase the exposure of active sites, effectively accelerate charge transfer, electrolyte diffusion, and gas release, and further elevate electrochemical performance. Liu et al. fabricated amorphous NiFe-based phosphides (NiFeP) with the morphology of nanoparticles, nanowires, nanosheets, or thick flakes and found that the morphologies of NiFeP samples showed a significant effect on their HER and OER performance for overall seawater splitting [38]. The highest HER activity was achieved on NiFeP nanosheets, while the best OER activity was attained on NiFeP nanowires. Density functional theory (DFT) calculations illustrated that the adsorption free energy difference between HO* and HOO* intermediates was reduced because of the incorporation of P atoms into NiFeOOH, which facilitated the OER kinetics. While the amorphous NiFeP demonstrated a very low H* adsorption energy close to 0 eV, which would efficiently enhance the HER activity.

Other than the deployment of experimental measures understanding the intrinsic catalytic mechanism and real active sites is of great importance in the rational design and application of NiFe-based TMPs. Since Liu and Rodriguez first predicted the comparable HER activity with the [NiFe] hydrogenase of Ni_2P(001) by DFT calculations [39], the research on catalytic mechanisms of NiFe-based TMPs for HER or OER has been intensively carried out but still in its infancy. The surface reconstructions under harsh test conditions make the catalytic mechanism too complex to track if just depending on the Tafel slope and DFT calculations [31]. Thus, to deeply trace the reaction mechanisms, the surface-active centers, and the nature of active species, the use of operando characterization techniques such as *in-situ* Raman measurement, *in-situ* Fourier transform infrared spectroscopy, and *in-situ* X-ray absorption spectroscopy, is highly required [40]. Although enormous efforts have been exerted to improve the catalytic performance of NiFe-based TMPs on HER and OER, and important progress has been made [29,30,41,42], however, there are still many challenges in obtaining NiFe-based TMPs electrocatalysts with high efficiency and especially long-term stability for practical application. Facile methods with good reproducibility and low cost are also very desirable for large-scale production of NiFe-based TMPs.

In recent years, constructing heterostructures has become an important and efficient strategy to improve the electrocatalytic properties of HER or OER [43–45]. For example, Sim and co-workers have synthesized a sulfur-rich Co-NiO heterostructure encapsulated on N-rich carbon nanofibers (SCNO@N-CNF) and found that the electrocatalyst exhibited low overpotentials of 247 mV and 169 mV at a current density of 10 mA cm^{-2} for OER and HER, respectively [46]. They attributed such excellent electrocatalytic performance to the improved conductivity, increased electrocatalytic active sites, and electron density at the heterostructures interfaces. Hao and colleagues just reported a NiFe-LDH/MoS_2 −Ni_3S_2/NF heterostructure catalyst, and this electrocatalyst delivered superior OER/HER activity and stability, and a low Tafel slope was also achieved [47]. These excellent electrocatalytic properties mainly resulted from the electronic structure modulation and synergistic effects between NiFe-LDH and MoS_2 −Ni_3S_2.

In the catalysts with heterostructures, owing to the unique structural merits, electrons can be rearranged at heterostructures interfaces, which can modulate the properties of active sites, and the synergistic interface effects can promote the reaction kinetics [43]. Thus, the heterostructure catalysts often show better activity on electrochemical water splitting than their counterparts with single-component. However, the research on heterostructure catalysts for water electrolysis mainly focuses on noble metal catalysts, transition metal oxides and hydroxides, and metal sulfide catalysts [48]. The investigation on heterostructured TMPs is still in its infancy stage. In this work, we designed and constructed heterostructures in NiFe phosphides, and the performance on HER, OER, and overall water splitting was systematically evaluated. The NiFeP/NF composite is synthesized by a wet chemical method under mild conditions followed by a chemical vapor phosphorization, which is facile, cost-efficient, environmentally benign, and reproducible. The electrochemical results manifest that the as-prepared NiFeP/NF composite is a valuable bifunctional catalyst with good catalytic activity and high stability. To reach the current densities of 10, 100, and 300 mA cm^{-2} for overall water splitting in an alkaline solution, the working potentials needed were 1.65, 1.84, and 2.03 V, accordingly. Long-term stability of 1100 h was achieved on NiFeP/NF when it was used as a bifunctional catalyst under a current density of 300 mA cm^{-2}. The good performance of NiFeP/NF makes it a promising bifunctional catalyst for water splitting under alkaline conditions. Such excellent performance on NiFeP/NF should be ascribed to (1) the synergistic effect promoted by the rich and diverse heterojunctions located in the NiFeP layer; (2) the intrinsic property of NiFe phosphides for fast electron transfer; (3) the good electric conductivity and robust structure of nickel foam. The good repeatability of the proposed method for producing NiFeP/NF has also been verified. The growth procedure of NiFe phosphides under mild conditions may provide a feasible method for preparing composites with rich heterostructures.

2. Experimental

2.1. Chemicals and materials

Nickel foam (NF) was commercially available from Changde Liyuan Material Co., Ltd. The thickness and porosity of the NF were 2 mm and 90 PPI, respectively. Nickel chloride hexahydrate ($NiCl_2{\cdot}6H_2O$, AR), iron sulfate heptahydrate ($FeSO_4{\cdot}7H_2O$, AR), urea (CH_4N_2O, ≥99.0%), and sodium hypophosphite monohydrate ($NaH_2PO_2{\cdot}H_2O$, AR) were purchased from Sinopharm Chemical Reagent Co., LTD, Shanghai, China. Potassium hydroxide (KOH) and iridium oxide powder (IrO_2, 99%) were bought from Meryer (Shanghai) Biochemical Technology Co., LTD. Pt/C powder (20% Pt) was from Alfa Aesar. All chemicals were used without further purification. DI water was used in all the experiments.

2.2. Preparation of NiFeP/NF

The commercial Ni foam was first cut into long sheets of 0.8 × 3 cm^2, cleaned successively in 1 M HCl, DI water, acetone, and ethanol for 15 min with ultrasonication, and then dried naturally. The nickel-iron hydroxides grown on nickel foam (denoted as NiFeOH/NF) were prepared according to a modified scheme reported in our previous work [49]. Briefly, 4 mmol $NiCl_2{\cdot}6H_2O$, 6 mmol $FeSO_4{\cdot}7H_2O$, and 20 mmol urea were first dissolved in 50 mL water to form a clear solution. Subsequently, the above solution was transferred into a glass bottle, and half of the NF was immersed. Next, the glass bottle was heated to 90 °C in an oil bath and reacted for 4 h. After cooling to room temperature, the sample was taken out. After rinsing with water several times, the sample was dried at 60 °C for 12 h. Then, NiFeOH/NF was acquired. Next, the phosphorization of NiFeOH/NF was conducted in a tube furnace under Ar gas flow. $NaH_2PO_2{\cdot}H_2O$ was used as the phosphating agent and placed separately at the upstream. To achieve the best electrocatalytic performance on HER or OER, the weight of $NaH_2PO_2{\cdot}H_2O$, reaction temperature, and time in the phosphating process were optimized. The corresponding electrochemical results are shown in Fig. S6. It can be concluded that the NiFe phosphide sample prepared under 3 g of sodium hypophosphite, 300 °C, and 2 h showed the best electrocatalytic activity on both HER and OER in 1 M KOH aqueous solution. For simplicity, we denote this selected sample as NiFeP/NF. With the same procedure, the samples of Ni or Fe phosphide on NF (named NiP/NF or FeP/NF) were also synthesized, except that only 10 mmol Ni^{2+} salt or 10 mmol Fe^{2+} salt was added into the precursor solution, respectively. It is noted that "NiFeOH/NF, NiFeP/NF, NiP/NF, and FeP/NF" were just the notations of composites and did not represent any stoichiometric compositions.

2.3. Materials Characterization

The X-ray diffraction (XRD) patterns were recorded on a Bruker-AXS D8 X-ray diffractometer with Cu K-alpha radiation. X-ray photoelectron spectroscopy (XPS) was performed on a Thermo Scientific Escalab-250Xi X-ray spectrometer at 150 W with an Al K-alpha X-ray source. The surface morphology analysis of the samples was conducted on a Hitachi S3400 scanning electron microscopy (SEM), and the energy dispersive X-ray spectroscopy (EDS) was collected on an Oxford X-MAX EDS system. Transmission electron microscopy (TEM) and selected area electron diffraction (SAED) were carried out on a Tecnai G2 F30/F20 JEOL-2100F TEM system at 200 kV. For the TEM observation, the samples were first sonicated in ethyl alcohol, and the dispersion was loaded on a copper grid. The HRTEM images were analyzed by Digital Micrograph.

2.4. Electrochemical measurements

The electrocatalytic performance was determined on a CHI 760E electrochemical workstation connected to a classic three-electrode cell containing 1.0 M KOH electrolyte. The NiFeP/NF sheet, a platinum sheet, and a Hg/HgO electrode (1 M NaOH) were used as the working, counter, and reference electrodes, respectively. The polarization curves were recorded with linear scan voltammogram (LSV) or cyclic voltammogram (CV) at a scan rate of 5 mV s^{-1}. In this work, to fix the geometric area of electrodes, all the NF-based electrodes were sealed with an insulating and chemically stable silicone resin, and the area was confined to 0.8 × 1 cm^2 (Fig. S1).

The electrochemical double-layer capacitance (C_{dl}) measurements were recorded in the potential range (−0.4 ~ −0.3 V) without faradic processes at scan rates of 10, 20, 40, 60, 80, and 100 mV s^{-1}. Electrochemical impedance spectra (EIS) were collected in a frequency range from 100 kHz to 10 mHz with an AC amplitude of 5 mV. The initial potential was set at the potential corresponding to the current density of 10 mA cm^{-2}. The catalytic stability was determined by chronopotentiometry. More experiment details can be found in the supporting information. All the electrode potentials are calibrated against a reversible hydrogen electrode (RHE) using the following equation:

$$E_{RHE} = E_{Hg/HgO} + (0.059pH + 0.098)\ V$$

where $\boldsymbol{E_{RHE}}$ is the potential referred to the RHE and $\boldsymbol{E_{Hg/HgO}}$ is the measured potential against the Hg/HgO reference electrode. To keep a relatively stable state on the interface of the electrode and the electrolyte, five CV cycles were swept before every measurement. All the electrochemical curves were corrected with 90% of the *iR* drop compensation.

3. Results and discussion

3.1. Synthesis and characterization of NiFeP/NF

To keep tight contact between the catalyst layer and NF and promote electron transport during the electrochemical processes, NiFeP was directly grown on Ni foam, which is of great importance in improving the catalytic performance. First, SEM images were used to demonstrate the morphology of NiFeOH/NF and NiFeP/NF. It can be found in Fig. 1a that dense free-standing sheets are formed on the NF after the wet chemical process. After phosphorization, the sheets in NiFeOH/NF completely disappeared and transformed into lots of flakes with random shapes. To determine the distribution of Ni, Fe, and P elements in NiFeP/NF, the EDS element mapping pictures were collected and depicted in Fig. 1c-g. The mapping results manifested the uniform distribution of Ni, Fe, and P elements in the NiFeP layer. Here, O element was also detected, which should be ascribed to the oxidation of NiFeP by exposure to ambient [50–52]. To study the structure of the samples, XRD patterns were determined and shown in Fig. 2a. In all the XRD curves, the three sharp peaks at about 44.9°, 52.4°, and 76.7° were from the Ni metal underneath (PDF # 01–1260). In the plot of NiFeOH/NF, the weak peaks at 11.58°, 23.25°, 34.44°, 39.2°, and 61.17° could be indexed to (003), (006), (012), (015), and (113) planes of NiFe layered double hydroxide (NiFe-LDH, PDF # 51–0463), which proved that a NiFe-LDH layer with short-range order and heterostructures was formed under the mild reaction conditions in the wet chemical process. Next, the XRD plots of the phosphides were analyzed. The peaks at 41.11°, 47.76°, 54.57°, 55.35°, and 74.91° in the XRD plot of NiP/NF are indexed as (111), (210), (002), (211), and (400) planes corresponding to the hexagonal phase of Ni_2P (PDF # 3–065–9706), while the peaks at 38.52° and 49.37° correspond to the cubic phase of Ni_7P_3 (PDF # 03–1101). In the XRD plot of FeP/NF the diffraction peaks at 36.44°, 47.76°, 49.59°, 69.07°, 47.48°, 63.14°, 41.2°7, 54.88°, and 57.76° are assigned to the planes of the orthorhombic phase of FeP (PDF # 1–089–4863), the hexagonal phase of Fe_2P (PDF # 1–083–2337), and the tetragonal phase of $FeNi_2P$ (PDF # 051–1367), accordingly. In the XRD pattern of NiFeP/NF, most of the diffraction peaks present in NiP/NF and FeP/NF could be found but became very weak, which meant the chemical combination of P atom further decreased the crystallinity and more

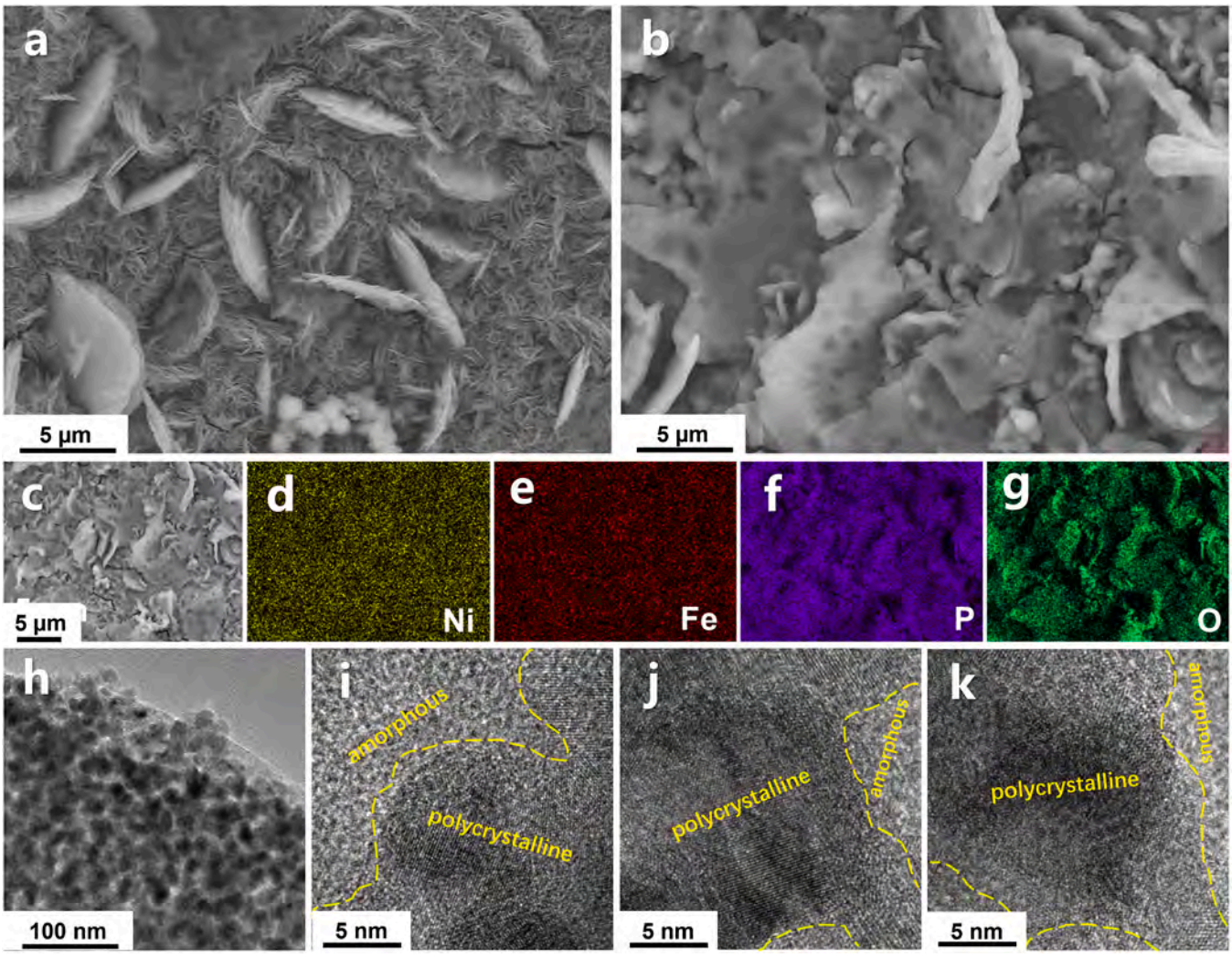

Fig. 1. SEM and TEM characterization of the samples of NiFeOH/NF and NiFeP/NF: a) SEM image of NiFeOH/NF, b) SEM image of NiFeP/NF, c-g) EDS elemental mapping pictures of NiFeP/NF, and h-k) TEM and HRTEM images of the NiFeP composite.

heterojunctions were formed in the NiFeP layer. When integrating mono Ni and Fe phosphides into the NiFeP compound, the mismatch in the crystalline phase and facets will produce external or internal defects and the electronic structure will be modulated in NiFeP, which will determine the adsorption/desorption of reactive intermediates, intrinsic activity, and stability [30,53]. For clarity, the attribution of the diffraction peaks from the phosphides is also listed in Table S1.

To better detect the microstructures, the TEM images of NiFeOH and NiFeP were taken and listed in Fig. 1 and Fig. S2. It can be found in Fig. S2a that NiFeOH was composed of many folded layers, and the HRTEM image (inset in Fig. S2a) clearly exhibited the microstructures with long-range disorder and short-range order. However, after the phosphorization process, the sheets of many interconnected nanoparticles were formed in the NiFeP layer (Fig. 1h and S2b). The HRTEM pictures obviously revealed the polycrystalline structures surrounded by adjacent amorphous domains in the NiFeP sheets (Fig. 1i-k). To better study the microstructures, the lattice fringes of the polycrystalline structures were examined and illustrated in Fig. S4a-c, and the interplanar spacings were consistent with the lattice planes of Ni_2P, FeP, Fe_2P, and NiFeP crystals, implying the coexistence of above phosphides in the NiFeP layer. Furthermore, the SAED pattern in Fig. S4d also well matched the phase indicators of hexagonal Ni_2P, cubic Ni_7P_3, orthorhombic FeP, hexagonal Fe_2P, and tetragonal $FeNi_2P$. Notably, the result from the TEM analysis was in good accordance with that from the XRD characterization. Thus, more complicated microstructures with low crystallinity were formed in the NiFeP layer, which first should be attributed to the formation of the polycrystals by slow co-deposition of Ni and Fe ions during the preparation of NiFe (hydro)oxides under mild conditions, and the unique polycrystal characteristic was retained in the NiFe phosphides after the phosphorization step. Such unique structures can create rich heterojunctions throughout the NiFeP composites layer, improving the exposure of higher active sites and promoting the reaction kinetics in the electrochemical process [54,55].

To investigate the surface element composition and valence state, XPS measurements were further conducted on NiFeOH/NF and NiFeP/NF. The XPS survey spectra in Fig. S3 clearly show the existence of Ni, Fe, and O elements in these two samples, while the P element is newly incorporated into NiFeP/NF. Then, the high-resolution XPS spectrum of Ni 2p in NiFeP/NF is deconvoluted into five main peaks (Fig. 2b). The peaks at 853.1, 856.4, and 874.1 eV correspond to the Ni $2p_{3/2}$ orbital of Ni-P, Ni $2p_{3/2}$ and Ni $2p_{1/2}$ of Ni-O [56–58], respectively. The related satellite peaks are at 861.5 (Ni 2p3/2) and 879.8 eV (Ni 2p1/2) [50]. In the Fe 2p spectrum (Fig. 2c), the peak pair located at the binding energy of 706.8 eV/719.9 eV (the blue lines) is attributed to Fe $2p_{3/2}$/Fe $2p_{1/2}$ for the Fe-P bond in the phosphides, and the peak pair at 710.8 eV/723.8 eV (the green lines) could be ascribed to Fe $2p_{3/2}$/Fe $2p_{1/2}$ of Fe^{2+} [59,60]. Moreover, the peak pair at 713.8 eV/725.9 eV (the purple lines) is assigned to Fe $2p_{3/2}$ /Fe $2p_{1/2}$ of Fe^{3+}. In the P 2p

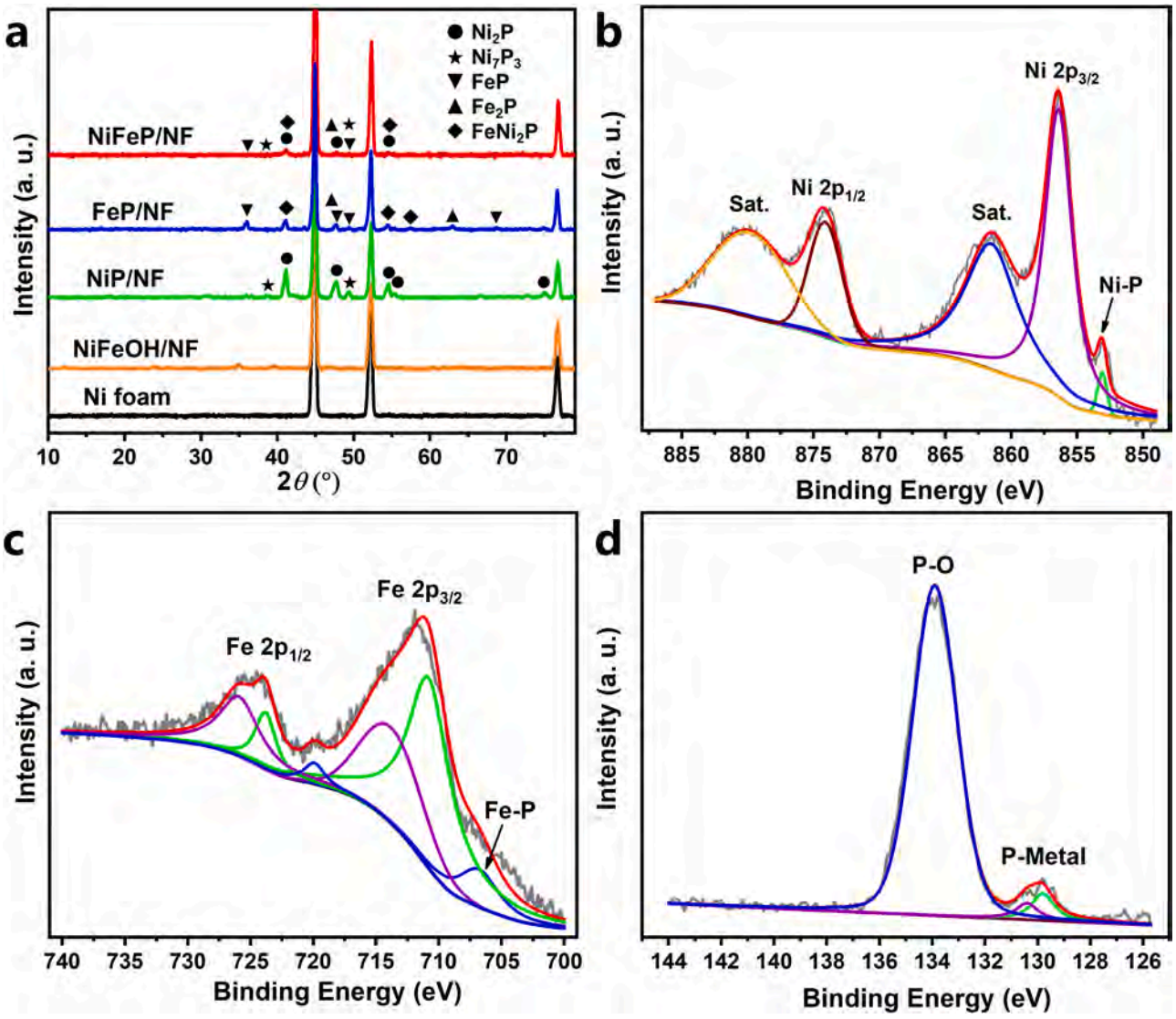

Fig. 2. a) XRD patterns of NF, NiFeOH/NF, NiP/NF, FeP/NF and NiFeP/NF; the detailed XPS spectra of Ni 2p b), Fe 2p c), and P 2p d) of NiFeP/NF.

XPS spectrum (Fig. 2d), the peaks at 129.8 and 130.4 eV are attributed respectively to P $2p_{3/2}$ and P $2p_{1/2}$ in P-metal bonds [61–63], which confirms the formation of NiFe phosphides. The strong peak of 133.9 eV is attributed to the P-O bond in PO_4^{3+} due to the surface oxidization when exposing NiFeP/NF to ambient [34,64], which is commonly observed for metal phosphides.

3.2. Electrocatalytic performance on HER

The HER electrocatalytic performance of different phosphides was first investigated in 1.0 M KOH aqueous solution. The HER performance of commercial Pt/C catalyst (20%) was also determined as the benchmark for comparison. The representative polarization curves are presented in Fig. 3a. To deliver the current densities of 10, 50, 100, and 300 mA cm^{-2}, the overpotentials needed on NiFeP/NF are 102, 174, 220, and 352 mV, respectively. These overpotential values were much lower than those on NiP/NF and FeP/NF (Fig. 3b) but still higher than those on Pt/C.

The performance of our NiFeP/NF is comparable to or better than that of recently reported phosphide HER catalysts (Table S2). In order to reveal the HER reaction kinetics of different catalysts, the Tafel plots were further evaluated in the low overpotential range (Fig. 3c). It can be clearly seen that the Tafel slope of Pt/C is the lowest (50.1 mV dec^{-1}), the second lower Tafel slope of NiFeP/NF is 101 mV dec^{-1} which was much smaller than that of NiP/NF (147.9 mV dec^{-1}) and FeP/NF (122.1 mV dec^{-1}), indicating the rapid HER reaction kinetics of NiFeP composite. Such improvement should be attributed to the heterojunctions and rich defects in the NiFeP composite, which can provide more active sites and promote the H* adsorption in the HER process [65]. The heterojunction structure can increase the carrier separation and transfer rate in the HER at the interface [66]. To get further insight into the HER activity, the EIS data were determined, and the fitted plots are shown in Fig. 3d. All Nyquist plots of the phosphides reveal similar semicircles corresponding to different charge transfer resistance (R_{ct}) values. The semicircles of FeP/NF and NiP/NF are more prominent than that of NiFeP/NF, implying a higher R_{ct} in the HER process. The fitted results are listed in Table S3. There was a slight difference in resistance (R_e) but a significant disparity among the R_{ct} values. The smallest R_{ct} value of 5.07 Ω was obtained on NiFeP/NF, implying its lowest charge transfer resistance at the electrode/electrolyte interface. The EIS results were in good consistence with the Tafel slopes of the samples, proving that the charge transfer kinetics played an important role in the process of HER. Electrocatalytic-activity-specific surface area (ECSA) is an important parameter reflecting the intrinsic electrochemical activity of catalysts. To determine the ECSA of different catalysts, CV measurement was performed in the non-Faradaic potential region, and the

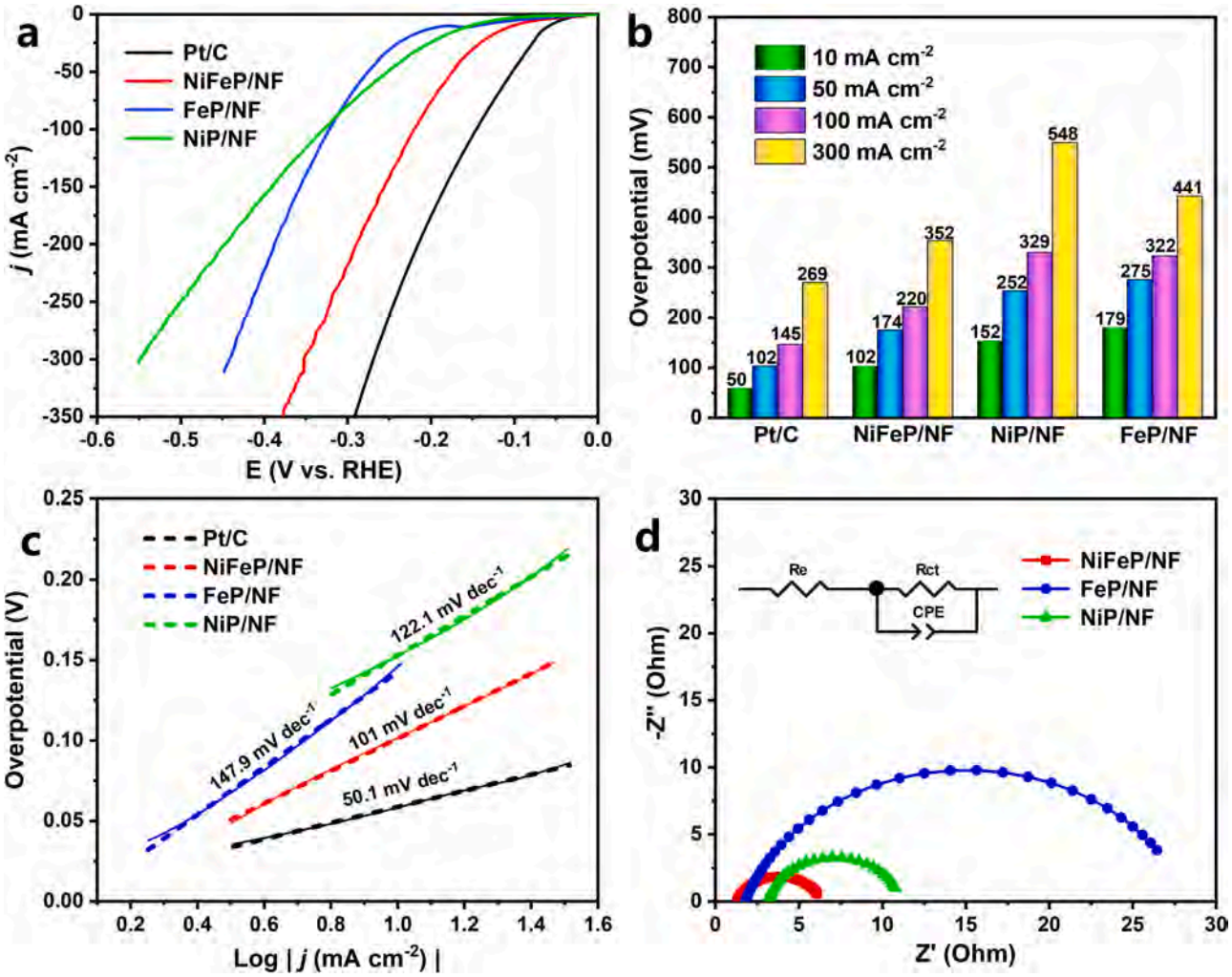

Fig. 3. HER catalytic performance of different phosphides: a) HER polarization curves, b) overpotential values at different current densities, c) Tafel slopes of NiP/NF, FeP/NF, NiFeP/NF, and Pt/C, and d) Nyquist plots of NiP/NF, FeP/NF, and NiFeP/NF. Inset in panel d is the electrical equivalent circuit used for fitting the Nyquist plot.

double-layer capacitance (C_{dl}) values are shown in Fig. S5 [67]. The largest C_{dl} value of 20.38 mF cm^{-1} was acquired for NiFeP/NF, which implied the largest electrochemical active surface area (ECSA) among all three phosphides, suggesting larger reactive space and more active sites for favorable electrode reactions. The above results confirm that both small charge transfer resistance and high active surface area were attained on NiFeP/NF, propelling outstanding electrocatalytic activity for HER. Also, the synergistic effects among Ni_2P, FeP, Fe_2P, and NiFeP phases in the NiFeP composite are vital for improving the HER catalytic performance of NiFeP/NF.

3.3. Electrocatalytic performance on OER

The OER performance of the phosphides was also investigated with cyclic voltammetry. In specific, to exclude the influence from the oxidation peaks of Ni^{2+} and Fe^{2+}, the backward segments of the CV curves were used for characterizing the OER activity. The polarization curves are depicted in Fig. 4a, and the IrO_2 catalyst was used as the benchmark. For comparison, the overpotential values under the typical current densities are listed in Fig. 4b. Strikingly, all the phosphides require lower overpotentials than the corresponding values on IrO_2 under the same current densities, implying better OER activity of NiP/NF, FeP/NF, and NiFeP/NF than that of IrO_2. Among the three TMPs, NiFeP/NF showed the best OER activity, and its overpotential values are 216, 239, and 253 mV under the corresponding current densities of 10, 50, and 100 mA cm^{-2}, which means a big improvement on OER catalytic activity for NiFeP/NF. Low overpotential values rank NiFeP/NF among the best phosphides for catalyzing OER, even better than the most promising NiFe double-layered hydroxide catalysts (Table S4). A small Tafel slope of 28.9 mV dec^{-1} in the low overpotential range was achieved on NiFeP/NF, indicating the favorable reaction kinetics for OER. Similarly, EIS was determined to study the OER activity further, and the fitted Nyquist plots are presented in Fig. 4d. All the TMP samples gave similar Nyquist plots with a semicircular shape, corresponding to the charge transfer resistance (R_{ct}). The fitting results are shown in Table S5, and all the R_e values of the TMP samples were less than 1.65 Ω, implying good electric conductivity and fast electron transmission during the OER process. The R_{ct} of NiFeP/NF was only 1.40 Ω, much smaller than FeP/NF and NiP/NF, thus leading to enhanced charge transfer and faster catalytic kinetics.

3.4. Electrocatalytic performance for overall water splitting

Given the good catalytic activity on both HER and OER, NiFeP/NF was then employed as a bifunctional catalyst for overall water splitting in a two-electrode electrolyzer containing 1 M KOH electrolyte (inset in Fig. 5c). For comparison, an electrolyzer of Pt/C/NF || IrO_2/NF was also assembled and tested under the same conditions. The polarization

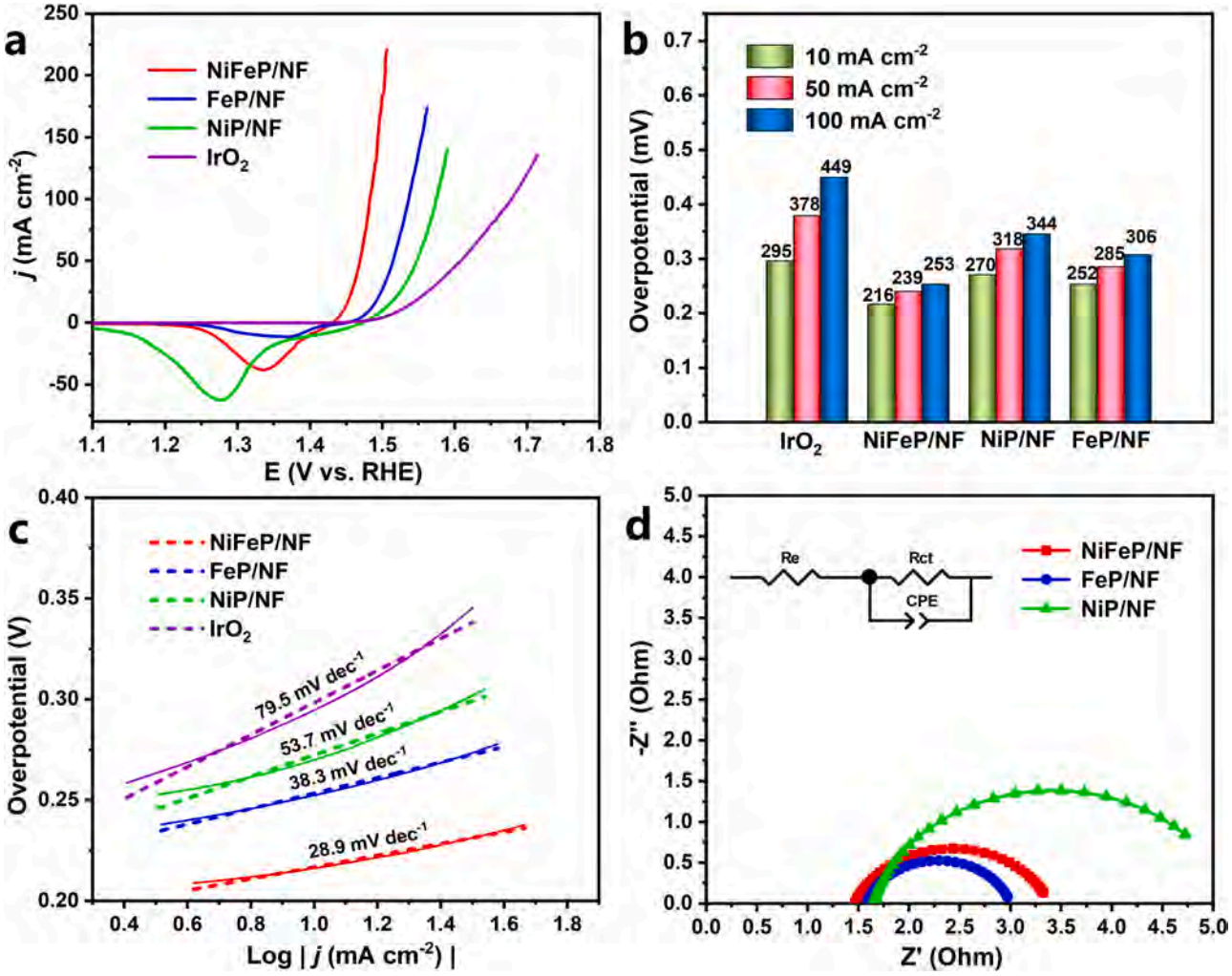

Fig. 4. OER electrocatalytic performance: a) OER polarization curves, b) overpotential values at different current densities, c) Tafel slopes of NiP/NF, FeP/NF, NiFeP/NF, and IrO_2, and d) Nyquist plots of NiP/NF, FeP/NF, and NiFeP/NF. Inset in panel d is the electrical equivalent circuit used for fitting the Nyquist plots.

curves for overall water splitting are shown in Fig. 5a. To deliver current densities of 10 and 100 mA cm^{-2}, the cell voltages needed on NiFeP/NF || NiFeP/NF were 1.65 and 1.84 V, respectively. In contrast, the corresponding cell voltages on Pt/C/NF || IrO_2/NF were 1.58 and 2.0 V, higher than that on NiFeP/NF || NiFeP/NF in the high potential range. The water-splitting voltage of NiFeP/NF || NiFeP/NF at 10 mA cm^{-2} is comparable to those on the metal phosphide-based bifunctional electrocatalysts reported recently (Table S6).

Good stability is also important for a qualified catalyst in commercial use. Therefore, the stability of NiFeP/NF on overall water splitting was inspected at a current density of 300 mA cm^{-2} by chronopotentiometry, and the curve is presented in Fig. 5c. Remarkably, after 1100 h of water electrolysis, the electrocatalytic activity was still well kept. The electrolytic voltage increased by 87 mV, manifesting the robust stability of NiFeP/NF, which is superior to most previously reported catalysts (Table S7). After the stability evaluation, the polarization curve was also recorded, and there was just a slight decay (Fig. 5a), further proving the robust catalytic stability of NiFeP/NF. From a practical aspect, Faradaic efficiency can exhibit the effectiveness of a catalyst in facilitating electrochemical water-splitting reactions. Then, the Faradaic efficiency of NiFeP/NF on overall water splitting was determined to be 95.7% by a drainage method, implying very high productivity on HER and OER (more details can be seen in the SI). Moreover, the repeatability of catalysts is also a key indicator for volume-produce. Next, the repeatability of NiFeP/NF was evaluated, and the result is exhibited in Fig. 5d. It can be seen that the CP curves showed good consistency, indicating good repeatability of the proposed preparation method. The details on the repeatability evaluation were described in the supporting information.

To better trace the changes of the used NiFeP/NF samples after 1100 h's water electrolysis, the methods of SEM, TEM, and XRD were employed to characterize the morphology, phase, microstructure, and element distribution and the results are shown in Fig. S7 and S8. It can be found from the SEM images (Fig. S7b,c) that there were remarkable changes in the morphology of the two electrodes after 1100 h of water electrolysis. The flakes presented in the as-prepared NiFe phosphides completely disappeared after the long-time hydrogen generation, and many microparticles with irregular shapes formed on the cathode (Fig. S7b), which should be attributed to the strong impact from the intense release of H_2 at the cathode surface under the high current density. While the anode was full of ravines and holes in microscale (Fig. S7c), it seemed that serious carving had happened at the anode surface due to the fast and longstanding emission of O_2. At the same time, a strong oxidizing atmosphere was well maintained at the anode/electrolyte interface under the co-function of the high electric potential and the newly produced oxygen species, which deeply reformed the morphology and changed the element distribution of the anode. The EDS spectra and elemental ratios of the two electrodes recorded by SEM area mapping are shown below the corresponding SEM images (Fig. S7d-f). Because of the additional signal generated from the Ni foam underneath,

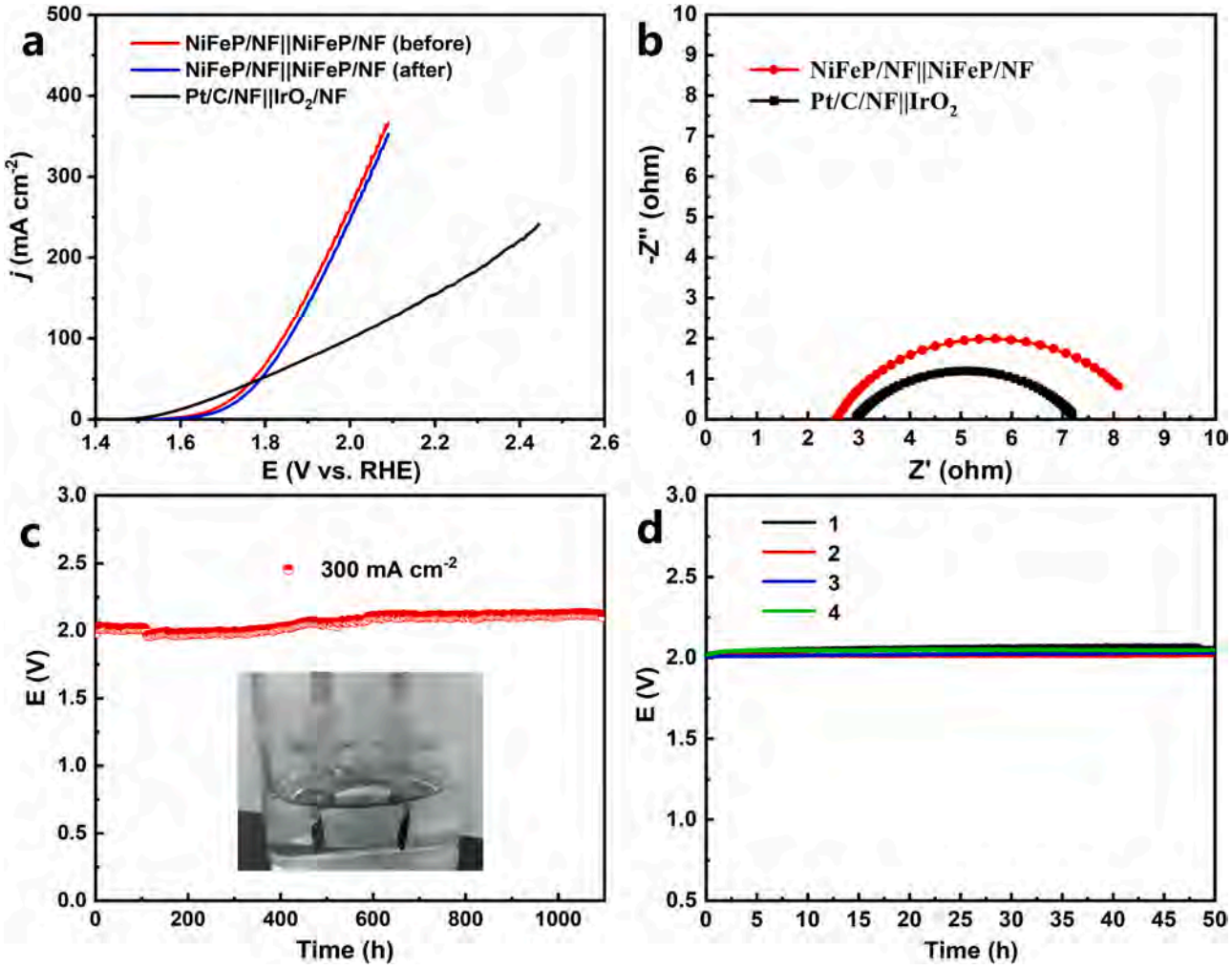

Fig. 5. Electrocatalytic performance for overall water splitting in 1.0 M KOH aqueous solution: a) LSV polarization curves and b) Nyquist plots of NiFeP/NF || NiFeP/NF, and Pt/C/NF || IrO_2/NF electrolyzers, c) chronopotentiometry curve of NiFeP/NF || NiFeP/NF electrolyzer under the current density of 300 mA cm^{-2} for 1100 h, and d) chronopotentiometry curves of 4 sets of NiFeP/NF || NiFeP/NF electrolyzers fabricated from different batches. The inset in panel **c** is the photograph of the two-electrode electrolytic cell.

the ratios of Ni elements were inaccurate. Thus, we just analyzed the variation of elemental ratios on O, P, and Fe. It can be concluded that the atomic ratio of O/P decreased from 1.61 in the as-prepared NiFeP/NF sample to 1.27 on the cathode after the long-time HER test, implying a decrease of O content, which could be ascribed to the strong reducing action at the cathode. On the contrary, there was a sharp increase to 57.8 in the atomic ratio of O/P on the anode, which obviously resulted from the extremely oxidizing atmosphere and the heavy oxidation of phosphides at the surficial layer of the anode. As for the change of Fe content on the two electrodes, there existed two opposite trends. The Fe content descended to a very low value on the anode, which meant the dissolution of Fe content from the anode into the electrolyte. However, the Fe content on the cathode was improved to a level higher than that in the as-prepared NiFeP/NF, which might be attributed to the re-deposition of the dissolved Fe ion from the anode. In other words, there was maybe Fe transfer from the anode to the cathode, and more proof were needed to ensure the existence of such a process. From the HRTEM images in Fig. S8, it could be observed that the heterostructures were still kept in the two electrodes after the 1100 h of stability test, but the degree of crystallinity became lower, especially for the anode, which was further proved by the corresponding SAED patterns (inset in Fig. S8a,b) and the XRD patterns (Fig. S8c).

The obtained NiFeP/NF catalyst exhibited excellent properties on HER, OER, and overall water splitting in both activity and stability. These improvements can be attributed to the unique heterostructures of NiFeP composites. Abundant heterojunctions are constructed between different phases of the NiFe phosphides, and the lattice strain at the heterojunction interface can expose higher active sites because of the rearrangement of the local electrons at the interfaces [68]. Meanwhile, the synergistic effect of different active sites can promote the kinetics, activity, and efficiency in the water-splitting process [69]. When NiFeP/NF is used as an OER electrocatalyst, the surface layer could be oxidized into the phosphides/oxides core-shell assembly, which affords catalytic sites for high OER activity [70]. Meanwhile, the phosphides can act as electric conductors for fast electron transfer from the active metal oxide shell [71]. As a result, the outer oxides and the inner phosphides construct a unique hybrid structure in which the co-function of oxides and phosphides may lead to a strong synergistic effect that greatly elevates the catalytic activity on OER.

4. Conclusion

In summary, we proposed a feasible method to prepare NiFe phosphide composite NF efficiently and cheaply. The obtained NiFeP/NF exhibited high electrocatalytic performance on both HER and OER because of its unique heterostructures and the synergistic effect of different phosphide phases in the NiFeP composite. Based on the heterostructures constructed among the polycrystalline and amorphous

surroundings in the NiFeP layer, abundant higher active sites are formed in the bulk and surface of the flakes, which would accelerate the charge transfer and promote the reaction kinetics in the HER or OER processes. Moreover, NiFeP/NF also has striking stability and good repeatability for overall water splitting, making it a very promising catalyst for water electrolysis. This work may provide a valuable route to prepare electrocatalysts with rich heterojunctions and high-efficiency performance.

CRediT authorship contribution statement

Guofa Dong: Project administration, Conceptualization, Methodology, Investigation, Writing-original draft. **Tingting Chen:** Data curation, Formal analysis, Validation. **Fengyan Xie:** Methodology, Software. **Jianrong Xia:** Resources. **Donglin XUE, Tingyan Liu, Long Chen, and Feng Xie:** Investigation. **Fengyun Wang**: Funding acquisition. **Shaowu Du:** Supervision, Funding acquisition, Writing - review & editing. **Johnny C. Ho:** Supervision, Project administration, review & editing.

Declaration of Competing Interest

The authors declare that they have no known competing financial interests or personal relationships that could have appeared to influence the work reported in this paper.

Data availability

Data will be made available on request.

Acknowledgments

This work was financially supported by the National Natural Science Foundation of China [grant numbers 21972060, 21805194]; the Natural Science Foundation of Fujian Province [grant numbers 2020J02046, 2022I0043, 2020J01852]; the Science and Technology Project of Fuzhou [grant numbers 2021-S-237, 2021-S-090]; the Science and Technology Project of Fuzhou Institute of Oceanography [grant number 2022F12]; the President's Fund of Minjiang University [grant number 103952022129]; and the Key Research and Development Program of Shandong Province [grant number 2019GGX102067].

Appendix A. Supporting information

Supplementary data associated with this article can be found in the online version at doi:10.1016/j.jallcom.2023.171746.

References

[1] L.J. Huang, H.J. Lin, H. Wang, L.Z. Ouyang, M. Zhu, Amorphous alloys for hydrogen storage, J. Alloy. Compd. 941 (2023), 168945, https://doi.org/10.1016/j.jallcom.2023.168945.
[2] S.Z. Zhiznin, N.N. Shvets, V.M. Timokhov, A.L. Gusev, Economics of hydrogen energy of green transition in the world and Russia.Part I, Int. J. Hydrog. Energy 48 (2023) 21544–21567, https://doi.org/10.1016/j.ijhydene.2023.03.069.
[3] M. Yue, H. Lambert, E. Pahon, R. Roche, S. Jemei, D. Hissel, Hydrogen energy systems: A critical review of technologies, applications, trends and challenges, Renew. Sustain Energy Rev. 146 (2021), 111180, https://doi.org/10.1016/j.rser.2021.111180.
[4] Z.P. Ifkovits, J.M. Evans, M.C. Meier, K.M. Papadantonakis, N.S. Lewis, Decoupled electrochemical water-splitting systems: a review and perspective, Energy Environ. Sci. 14 (2021) 4740–4759, https://doi.org/10.1039/D1EE01226F.
[5] N. Shang, Z. Wang, S. Liu, S. Ma, Y. Xing, X. Cheng, W. Gao, S. Gao, C. Wang, Constructing hierarchical structure electrocatalyst for efficient hydrogen evolution and selective oxidation of benzylamine, J. Alloy. Compd. 912 (2022), 165259, https://doi.org/10.1016/j.jallcom.2022.165259.
[6] H. Wu, Q. Huang, Y. Shi, J. Chang, S. Lu, Electrocatalytic water splitting: Mechanism and electrocatalyst design, Nano Res. (2023) 5502–5508, https://doi.org/10.1007/s12274-023-5502-8.
[7] X. Luo, X. Tan, P. Ji, L. Chen, J. Yu, S. Mu, Surface reconstruction-derived heterostructures for electrochemical water splitting, EnergyChem 5 (2023), 100091, https://doi.org/10.1016/j.enchem.2022.100091.
[8] H. Zhang, Y. Luo, P.K. Chu, Q. Liu, X. Liu, S. Zhang, J. Luo, X. Wang, G. Hu, Recent advances in non-noble metal-based bifunctional electrocatalysts for overall seawater splitting, J. Alloy. Compd. 922 (2022), 166113, https://doi.org/10.1016/j.jallcom.2022.166113.
[9] W. Xiong, H. Yin, T. Wu, H. Li, Challenges and opportunities of transition metal oxides as electrocatalysts, Chem. – A Eur. J. 29 (2023), e202202872, https://doi.org/10.1002/chem.202202872.
[10] M. Chen, N. Kitiphatpiboon, C. Feng, A. Abudula, Y. Ma, G. Guan, Recent progress in transition-metal-oxide-based electrocatalysts for the oxygen evolution reaction in natural seawater splitting: A critical review, eScience 3 (2023), 100111, https://doi.org/10.1016/j.esci.2023.100111.
[11] K. Bhunia, S. Khilari, M. Chandra, D. Pradhan, S.-J. Kim, Carbon nitride anchored NiO nanoparticles as robust catalyst for electrochemical oxygen evolution reaction, J. Alloy. Compd. 935 (2023), 167842, https://doi.org/10.1016/j.jallcom.2022.167842.
[12] S. Kumaravel, K. Karthick, S.S. Sankar, A. Karmakar, R. Madhu, K. Bera, S. Kundu, Current progressions in transition metal based hydroxides as bi-functional catalysts towards electrocatalytic total water splitting, Sustain. Energy Fuels 5 (2021) 6215–6268, https://doi.org/10.1039/D1SE01193F.
[13] E.W.Qianfeng Liu, Gongquan Sun, Layered transition-metal hydroxides for alkaline hydrogen evolution reaction, Chin. J. Catal. 41 (2020) 574–591, https://doi.org/10.1016/s1872-2067(19)63458-3.
[14] Y. Liu, Y. Guo, Y. Liu, Z. Wei, K. Wang, Z. Shi, A mini review on transition metal chalcogenides for electrocatalytic water splitting: bridging material design and practical application, Energy Fuels 37 (2023) 2608–2630, https://doi.org/10.1021/acs.energyfuels.2c03833.
[15] T. Zhang, J. Sun, J. Guan, Self-supported transition metal chalcogenides for oxygen evolution, Nano Res. 5676 (2023), 5670, https://doi.org/10.1007/s12274-023-5670-6.
[16] G. Janani, S. Surendran, H. Choi, T.-Y. An, M.-K. Han, S.-J. Song, W. Park, J.K. Kim, U. Sim, Anchoring of Ni12P5 microbricks in nitrogen- and phosphorus-enriched carbon frameworks: engineering bifunctional active sites for efficient water-splitting systems, ACS Sustain. Chem. Eng. 10 (2022) 1182–1194, https://doi.org/10.1021/acssuschemeng.1c06514.
[17] D. Liu, G. Xu, H. Yang, H. Wang, B.Y. Xia, Rational design of transition metal phosphide-based electrocatalysts for hydrogen evolution, Adv. Funct. Mater. 33 (2023) 2208358, https://doi.org/10.1002/adfm.202208358.
[18] S.H. Li, M.Y. Qi, Z.R. Tang, Y.J. Xu, Nanostructured metal phosphides: from controllable synthesis to sustainable catalysis, Chem. Soc. Rev. 50 (2021) 7539–7586, https://doi.org/10.1039/D1CS00323B.
[19] H.-M. Zhang, J.-J. Wang, Y. Meng, F. Lu, M. Ji, C. Zhu, J. Xu, J. Sun, Review on intrinsic electrocatalytic activity of transition metal nitrides on HER, Energy Mater. Adv. 2022 (2022), 0006, https://doi.org/10.34133/energymatadv.0006.
[20] L. Lin, S. Piao, Y. Choi, L. Lyu, H. Hong, D. Kim, J. Lee, W. Zhang, Y. Piao, Nanostructured transition metal nitrides as emerging electrocatalysts for water electrolysis: status and challenges, EnergyChem 4 (2022), 100072, https://doi.org/10.1016/j.enchem.2022.100072.
[21] H. Wang, S. Zhu, J. Deng, W. Zhang, Y. Feng, J. Ma, Transition metal carbides in electrocatalytic oxygen evolution reaction, Chin. Chem. Lett. 32 (2021) 291–298, https://doi.org/10.1016/j.cclet.2020.02.018.
[22] P. Chen, J. Ye, H. Wang, L. Ouyang, M. Zhu, Recent progress of transition metal carbides/nitrides for electrocatalytic water splitting, J. Alloy. Compd. 883 (2021), 160833, https://doi.org/10.1016/j.jallcom.2021.160833.
[23] C. Li, H. Zhang, M. Liu, F.-F. Lang, J. Pang, X.-H. Bu, Recent progress in metal–organic frameworks (MOFs) for electrocatalysis, Ind. Chem. Mater. 1 (2023) 9–38, https://doi.org/10.1039/D2IM00063F.
[24] Y. Peng, S. Sanati, A. Morsali, H. García, Metal–organic frameworks as electrocatalysts, Angew. Chem. Int. Ed. 62 (2023), e202214707, https://doi.org/10.1002/anie.202214707.
[25] D. Li, H. Liu, L. Feng, A review on advanced FeNi-based catalysts for water splitting reaction, Energy Fuels 34 (2020) 13491–13522, https://doi.org/10.1021/acs.energyfuels.0c03084.
[26] L. Sun, Q. Luo, Z. Dai, F. Ma, Material libraries for electrocatalytic overall water splitting, Coord. Chem. Rev. 444 (2021), 214049, https://doi.org/10.1016/j.ccr.2021.214049.
[27] H. Zhang, A.W. Maijenburg, X. Li, S.L. Schweizer, R.B. Wehrspohn, Bifunctional heterostructured transition metal phosphides for efficient electrochemical water splitting, Adv. Funct. Mater. 30 (2020) 2003261, https://doi.org/10.1002/adfm.202003261.
[28] T.O. Ogundipe, L. Shen, Yan Shi, Z. Lu, C. Yan, Recent advances on bimetallic transition metal phosphides for enhanced hydrogen evolution reaction, ChemistrySelect 7 (2022), e202200291, https://doi.org/10.1002/slct.202200291.
[29] W. Zhang, D. Li, L. Zhang, X. She, D. Yang, NiFe-based nanostructures on nickel foam as highly efficiently electrocatalysts for oxygen and hydrogen evolution reactions, J. Energy Chem. 39 (2019) 39–53, https://doi.org/10.1016/j.jechem.2019.01.017.
[30] Y. Chu, D. Wang, X. Shan, C. Liu, W. Wang, N. Mitsuzaki, Z. Chen, Activity engineering to transition metal phosphides as bifunctional electrocatalysts for efficient water-splitting, Int. J. Hydrog. Energy 47 (2022) 38983–39000, https://doi.org/10.1016/j.ijhydene.2022.09.070.
[31] Y. Zeng, M. Zhao, Z. Huang, W. Zhu, J. Zheng, Q. Jiang, Z. Wang, H. Liang, Surface reconstruction of water splitting electrocatalysts, Adv. Energy Mater. 12 (2022) 2201713, https://doi.org/10.1002/aenm.202201713.
[32] Z. Zhai, G. Jia, Y. Wang, X. Chen, Z. Zhang, Recent advances of anion regulated NiFe-based electrocatalysts for water oxidation, Sustain. Energy Fuels 5 (2021) 6298–6309, https://doi.org/10.1039/D1SE01535D.
[33] T. Chen, B. Li, K. Song, C. Wang, J. Ding, E. Liu, B. Chen, F. He, Defect-activated surface reconstruction: mechanism for triggering the oxygen evolution reaction

activity of NiFe phosphide, J. Mater. Chem. A 10 (2022) 22750–22759, https://doi.org/10.1039/D2TA04879E.
[34] X. Long, J. Meng, J. Gu, L. Ling, Q. Li, N. Liu, K. Wang, Z. Li, Interfacial engineering of NiFeP/NiFe-LDH heterojunction for efficient overall water splitting, Chin. J. Struct. Chem. 41 (2022) 2204046–2204053, https://doi.org/10.14102/j.cnki.0254-5861.2022-0048.
[35] S. Kumaravel, K. Karthick, S. Sam Sankar, A. Karmakar, R. Madhu, K. Bera, S. Kundu, Recent progresses in engineering of Ni and Co based phosphides for effective electrocatalytic water splitting, ChemElectroChem 8 (2021) 4638–4685, https://doi.org/10.1002/celc.202100984.
[36] A. Ray, S. Sultana, L. Paramanik, K.M. Parida, Recent advances in phase, size, and morphology-oriented nanostructured nickel phosphide for overall water splitting, J. Mater. Chem. A 8 (2020) 19196–19245, https://doi.org/10.1039/D0TA05797E.
[37] Y. Zhou, H.J. Fan, Progress and challenge of amorphous catalysts for electrochemical water splitting, ACS Mater. Lett. 3 (2021) 136–147, https://doi.org/10.1021/acsmaterialslett.0c00502.
[38] J. Liu, X. Liu, H. Shi, J. Luo, L. Wang, J. Liang, S. Li, L.-M. Yang, T. Wang, Y. Huang, Q. Li, Breaking the scaling relations of oxygen evolution reaction on amorphous NiFeP nanostructures with enhanced activity for overall seawater splitting, Appl. Catal. B Environ. 302 (2022), 120862, https://doi.org/10.1016/j.apcatb.2021.120862.
[39] P. Liu, J.A. Rodriguez, Catalysts for hydrogen evolution from the [NiFe] hydrogenase to the Ni_2P(001) surface: the importance of ensemble effect, J. Am. Chem. Soc. 127 (2005) 14871–14878, https://doi.org/10.1021/ja0540019.
[40] Y. AlSalka, S. Schwabe, J. Geweke, G. Ctistis, H. Wackerbarth, Electrochemical and photoelectrochemical water splitting: operando raman and fourier transform infrared spectroscopy as useful probing techniques, Energy Technol. 11 (2023) 2200788, https://doi.org/10.1002/ente.202200788.
[41] Q. Han, Y. Luo, J. Li, X. Du, S. Sun, Y. Wang, G. Liu, Z. Chen, Efficient NiFe-based oxygen evolution electrocatalysts and origin of their distinct activity, Appl. Catal. B: Environ. 304 (2022), 120937, https://doi.org/10.1016/j.apcatb.2021.120937.
[42] J. Zhao, J.-J. Zhang, Z.-Y. Li, X.-H. Bu, Recent progress on NiFe-based electrocatalysts for the oxygen evolution reaction, Small 16 (2020) 2003916, https://doi.org/10.1002/smll.202003916.
[43] Q. Quan, J.C. Ho, Recent advances in the construction of 2D heterostructures for electrocatalytic water splitting, Adv. Energy Sustain. Res. 3 (2022) 2200059, https://doi.org/10.1002/aesr.202200059.
[44] H. Choi, S. Surendran, Y. Sim, M. Je, G. Janani, H. Choi, J.K. Kim, U. Sim, Enhanced electrocatalytic full water-splitting reaction by interfacial electric field in 2D/2D heterojunction, Chem. Eng. J. 450 (2022), 137789, https://doi.org/10.1016/j.cej.2022.137789.
[45] J. Hao, K. Wu, C. Lyu, Y. Yang, H. Wu, J. Liu, N. Liu, W.-M. Lau, J. Zheng, Recent advances in interface engineering of Fe/Co/Ni-based heterostructure electrocatalysts for water splitting, Mater. Horiz. 10 (2023) 2312–2342, https://doi.org/10.1039/D3MH00366C.
[46] S. Surendran, S.C. Jesudass, G. Janani, J.Y. Kim, Y. Lim, J. Park, M.-K. Han, I. S. Cho, U. Sim, Sulphur assisted nitrogen-rich CNF for improving electronic interactions in Co-NiO heterostructures toward accelerated overall water splitting, Adv. Mater. Technol. 8 (2023), 2200572, https://doi.org/10.1002/admt.202200572.
[47] S. Wang, X. Ning, Y. Cao, R. Chen, Z. Lu, J. Hu, J. Xie, A. Hao, Construction of an advanced NiFe-LDH/MoS_2–Ni_3S_2/NF heterostructure catalyst toward efficient electrocatalytic overall water splitting, Inorg. Chem. 62 (2023) 6428–6438, https://doi.org/10.1021/acs.inorgchem.3c00425.
[48] Z. Li, M. Hu, P. Wang, J. Liu, J. Yao, C. Li, Heterojunction catalyst in electrocatalytic water splitting, Coord. Chem. Rev. 439 (2021), 213953, https://doi.org/10.1016/j.ccr.2021.213953.
[49] G. Dong, F. Xie, F. Kou, T. Chen, F. Wang, Y. Zhou, K. Wu, S. Du, M. Fang, J.C. Ho, NiFe-layered double hydroxide arrays for oxygen evolution reaction in fresh water and seawater, Mater. Today Energy 22 (2021), 100883, https://doi.org/10.1016/j.mtener.2021.100883.
[50] C. Wu, P. Kopold, P.A. van Aken, J. Maier, Y. Yu, High performance graphene/Ni_2P hybrid anodes for lithium and sodium storage through 3D yolk–shell-like nanostructural design, Adv. Mater. 29 (2017) 1604015, https://doi.org/10.1002/adma.201604015.
[51] I. Zafiropoulou, K. Papagelis, N. Boukos, A. Siokou, D. Niarchos, V. Tzitzios, Chemical synthesis and self-assembly of hollow Ni/Ni_2P hybrid nanospheres, J. Phys. Chem. C. 114 (2010) 7582–7585, https://doi.org/10.1021/jp910160g.
[52] P. Wang, Y. Luo, G. Zhang, M. Wu, Z. Chen, S. Sun, Z. Shi, MnOx-decorated nickel-iron phosphides nanosheets: interface modifications for robust overall water splitting at ultra-high current densities, Small 18 (2022) 2105803, https://doi.org/10.1002/smll.202105803.
[53] J. Yu, Q. Li, Y. Li, C.-Y. Xu, L. Zhen, V.P. Dravid, J. Wu, Ternary metal phosphide with triple-layered structure as a low-cost and efficient electrocatalyst for bifunctional water splitting, Adv. Funct. Mater. 26 (2016) 7644–7651, https://doi.org/10.1002/adfm.201603727.
[54] Y. Du, B. Li, G. Xu, L. Wang, Recent advances in interface engineering strategy for highly-efficient electrocatalytic water splitting, InfoMat 5 (2023), e12377, https://doi.org/10.1002/inf2.12377.
[55] L. Ji, Y. Wei, P. Wu, M. Xu, T. Wang, S. Wang, Q. Liang, T.J. Meyer, Z. Chen, Heterointerface engineering of Ni_2P–Co_2P nanoframes for efficient water splitting, Chem. Mater. 33 (2021) 9165–9173, https://doi.org/10.1021/acs.chemmater.1c02609.
[56] R. Bernasconi, M.I. Khalil, C. Iaquinta, C. Lenardi, L. Nobili, L. Magagnin, Nickel phosphides fabricated through a codeposition–annealing technique as low-cost electrocatalytic layers for efficient hydrogen evolution reaction, ACS Appl. Energy Mater. 3 (2020) 6525–6535, https://doi.org/10.1021/acsaem.0c00733.
[57] Y. Pan, Y. Liu, J. Zhao, K. Yang, J. Liang, D. Liu, W. Hu, D. Liu, Y. Liu, C. Liu, Monodispersed nickel phosphide nanocrystals with different phases: synthesis, characterization and electrocatalytic properties for hydrogen evolution, J. Mater. Chem. A 3 (2015) 1656–1665, https://doi.org/10.1039/C4TA04867A.
[58] B. Zhang, Y.H. Lui, H. Ni, S. Hu, Bimetallic $(Fe_xNi_{1-x})_2P$ nanoarrays as exceptionally efficient electrocatalysts for oxygen evolution in alkaline and neutral media, Nano Energy 38 (2017) 553–560, https://doi.org/10.1016/j.nanoen.2017.06.032.
[59] J. Masud, S. Umapathi, N. Ashokaan, M. Nath, Iron phosphide nanoparticles as an efficient electrocatalyst for the OER in alkaline solution, J. Mater. Chem. A 4 (2016) 9750–9754, https://doi.org/10.1039/C6TA04025J.
[60] C. Qian, F. Kim, L. Ma, F. Tsui, P. Yang, J. Liu, Solution-phase synthesis of single-crystalline iron phosphide nanorods/nanowires, J. Am. Chem. Soc. 126 (2004) 1195–1198, https://doi.org/10.1021/ja038401c.
[61] S. Cartagena, F.E. Bedoya Lora, J.A. Calderón, Enhancement of anodically treated stainless steel by NiFeP-catalyst electrodeposition as bifunctional electrodes for water electrolysis, J. Electrochem. Soc. 169 (2022), 044501, https://doi.org/10.1149/1945-7111/ac5ff1.
[62] H. Wang, S. Tao, Fabrication of a porous NiFeP/Ni electrode for highly efficient hydrazine oxidation boosted H_2 evolution, Nanoscale Adv. 3 (2021) 2280–2286, https://doi.org/10.1039/D1NA00043H.
[63] F. Diao, W. Huang, G. Ctistis, H. Wackerbarth, Y. Yang, P. Si, J. Zhang, X. Xiao, C. Engelbrekt, Bifunctional and self-supported NiFeP-layer-coated NiP rods for electrochemical water splitting in alkaline solution, ACS Appl. Mater. Interfaces 13 (2021) 23702–23713, https://doi.org/10.1021/acsami.1c03089.
[64] N. Jiang, B. You, M. Sheng, Y. Sun, Electrodeposited cobalt-phosphorous-derived films as competent bifunctional catalysts for overall water splitting, Angew. Chem. Int. Ed. 54 (2015) 6251–6254, https://doi.org/10.1002/anie.201501616.
[65] J.L. Fenton, B.C. Steimle, R.E. Schaak, Tunable intraparticle frameworks for creating complex heterostructured nanoparticle libraries, Science 360 (2018) 513–517, https://doi.org/10.1126/science.aar5597.
[66] S. Yang, Y. Wang, H. Zhang, Y. Zhang, L. Liu, L. Fang, X. Yang, X. Gu, Y. Wang, Unique three-dimensional Mo_2C@MoS_2 heterojunction nanostructure with S vacancies as outstanding all-pH range electrocatalyst for hydrogen evolution, J. Catal. 371 (2019) 20–26, https://doi.org/10.1016/j.jcat.2019.01.020.
[67] J. Zhang, L. Yu, Y. Chen, X.F. Lu, S. Gao, X.W. Lou, Designed formation of double-shelled Ni–Fe layered-double-hydroxide nanocages for efficient oxygen evolution reaction, Adv. Mater. 32 (2020) 1906432, https://doi.org/10.1002/adma.201906432.
[68] A. Li, X. Chang, Z. Huang, C. Li, Y. Wei, L. Zhang, T. Wang, J. Gong, Thin heterojunctions and spatially separated cocatalysts to simultaneously reduce bulk and surface recombination in photocatalysts, Angew. Chem. Int. Ed. 55 (2016) 13734–13738, https://doi.org/10.1002/anie.201605666.
[69] A. Wu, Y. Xie, H. Ma, C. Tian, Y. Gu, H. Yan, X. Zhang, G. Yang, H. Fu, Integrating the active OER and HER components as the heterostructures for the efficient overall water splitting, Nano Energy 44 (2018) 353–363, https://doi.org/10.1016/j.nanoen.2017.11.045.
[70] S. Jin, Are metal chalcogenides, nitrides, and phosphides oxygen evolution catalysts or bifunctional catalysts? ACS Energy Lett. 2 (2017) 1937–1938, https://doi.org/10.1021/acsenergylett.7b00679.
[71] Y. Li, R. Li, D. Wang, H. Xu, F. Meng, D. Dong, J. Jiang, J. Zhang, M. An, P. Yang, A review: Target-oriented transition metal phosphide design and synthesis for water splitting, Int. J. Hydrog. Energy 46 (2021) 5131–5149, https://doi.org/10.1016/j.ijhydene.2020.11.030.